Eur. Phys. J. C manuscript No.
(will be inserted by the editor)

Physics potential for the measurement of the H→ZZ decay at the CEPC (temporal title)

Ryuta Kiuchi[1], Yanxi Gu[2], Zhong Min[2], Shih-Chieh Hsu[3], Xin Shi[1], Kaili Zhang[1], Person XXX, Person YYY,,,

[1]Institude of High Energy Physics, Chinese Academy of Science, Beijing 100049, China
[2]Department of Modern Physics, University of Science and Technology of China, Hefei, China
[3]Department of Physics, University of Washington, Seattle 98195-1560, USA

Received: date / Accepted: date

Abstract The precision of the yield of the Higgs boson decaying into two Z bosons process at the Circular Electron-Positron Collider (CEPC) is evaluated. Including the recoil Z boson with the Higgsstrahlung process, total three Z bosons involves for this channel, from which decay combinations having a pair of leptons, quarks, and neutrinos are chosen and analyzed. A short discussion about the precision of the Higgs boson width is presented when the obtained precision of σ_{ZH}·Br(H→ZZ) is assumed.

Keywords First keyword · Second keyword · More

1 Introduction

After the discovery of the Higgs boson **??**, efforts are performed on measureing properties of the Higgs boson. One of motivations of these studies is to obtain hints for physics beyond the standard model (BSM) , whose existence is suggested by several experiment facts, such as dark matter, cosmological baryon-antibaryon asymmetry. The Circular Electron-Positron Collider (CEPC) is a proposed future circular e^+e^- collider, having its main ring circumstance of ∼100 km. As a Higgs factory, the CEPC is planned to operate at $\sqrt{s} = 240$ GeV with the integrated luminosity of $5.6ab^{-1}$ which is expected to achieve an order of magniutude improvement on measuremernts of Higgs boson properties as compared to the final LHC precision.

The Higgs boson production processes at $\sqrt{s} = 240$ GeV mainly consist of $e^+e^-\to ZH$ (Higgsstrahlung, hereafter, denote it as the ZH process) and $e^+e^-\to\nu_e\bar{\nu}_eH$ ($\nu_e\bar{\nu}_eH$ process), where the former is the dominant reaction and is going to be used for the best measurement of the cross section $\sigma(ZH)$ using the recoil mass method against the Z boson. That Z boson also serves as a tag of the ZH process. With help of this tag information, indivisual decay channels from the Higgs boson will be explored and give us valuable information on the Higgs boson properties ever, such as the branching ratios and its precisions.

The Higgs decay into a pair of Z bosons, via the ZH process, will be studied at the CEPC. Like the other decay modes, the Branching ratio $BR(H\to ZZ)$ can be estimated from the measurement of the signal yield, $\sigma(ZH)\times BR(H\to ZZ)$. In addition, the Higgs boson width Γ_H can be inferred. Under the assumption that the coupling structure follows to that of the SM, the branching ratio is proportional to the ratio, $BR(H\to ZZ) = \Gamma(H\to ZZ)/\Gamma_H \sim g^2_{HZZ}/\Gamma_H$, therefore, Γ_H is deduced with the precision of the coupling g^2_{HZZ} and the signal yield.

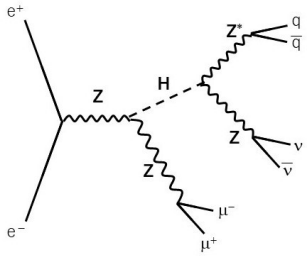

Fig. 1 Example Feynman diagram for Higgs boson production with decay into ZZ*, where 3 Z bosons are decaying into a pair of muons, quarks and neutrinos that is the signature of signal channels. It is a test version and should be updated .

[a]e-mail: shixin@ihep.ac.cn
[b]

Explanation about signal channels.

In this article, we present the relative accuracy of the measurement of the $H \to ZZ$ at the CEPC, based on the Monte Carlo (MC) simulation and data samples for the CEPC-v4 detector concept at $\sqrt{s} = 240$ GeV. In Section 2, we briefly introduce the CEPC detector design and the MC simulation. The detail of the data analysis are explained in Section 3, followed by the results and discussions in Section 4.

2 Detector design and simulation samples

The CEPC will hosts two interaction points (IP) on the main ring, where the detectors at each IP should record collision data under different center of mass energies varying from $\sqrt{s} = 91.2$ GeV as a Z factory to $\sqrt{s} = 240$ GeV as a Higgs factory. To fulfill those physics programs, a baseline concept is developed that is based on the ILC concept ref with further optimizations for the CEPC environment. List it from the most inner subdetector component, the detector concept is composed of a silicon vertex detector, a silicon inner tracker consisting of micro strip detectors, a Time Projection Chamber (TPC), a silicon external tracker, ultra-fine segmented calorimeters, an Electronmagnetic CALorimeter (ECAL) and an Hadronic CALorimeter (HCAL), a 3T superconducting solenoid, and a muon detector ref.

The CEPC simulation software package implements the baseline concept detector geometry. Events for the SM processes are generated by the Whizard ref including the Higgs boson signal, where the detector configuration and response is handled by the MokkaPlus ref. Modules for digitization of the signals at each sub detector creates the hit information. The reconstruction procedure

3 Analysis of HZZ decay modes

As briefly introduced in the Section 1, the analysis is focusing on signal channels where the decay products from three Z bosons are combinations of a pair of muons, a pair of jets and a pair of neutrinos. Distinguishing the status of the decay pairs from a on-shell Z boson and that from a off-shell Z boson, where both Z bosons are coming from the Higgs decay, the analysis comprises total 6 channels. For the convenience, we adopt following notation for each signal: $\mu\mu$H$\nu\nu qq$ represents $e^+e^- \to ZH \to Z(\to \mu\mu)H, H \to ZZ* \to Z(\to \nu\nu)Z*(\to qq)$. Note that both of Z bosons from a Higgs boson could have their invariant masses well lower than the nomial mass (∼91.2 GeV) kinematically, the Z boson having larger invariant mass is considered as *on-shell* Z boson here.

3.1 Event selection

Event selection is performed in several stages. The preselection builds higher-level objects, such as isolated muons, jets, and missing momentum from the particle flow objects reconstructed by the Arbor. The isolation requirements on muons, identified by the PF, are imposed, which is a threshold on the ratio between a sumation of energy in a volume defined by a cone of angular radius $R = 0.3$? (need to check the number) and the energy of the muon. Jets are clustered from the PFs but except isolated lepton candidates, using the k_t algorithm for the e^+e^- collision ($ee - kt$) with the FastJet package. Exclusive requirement ($N_{jet} = 2$) on number of jets is imposed. The events containing a positive charged muon and a negative charged muon with succesive jet clustering are kept for the latter part of the event selection.

At the next stage, the signal to background ratio is minimized by the set of selection criteria listed in the followings:

- M_{dimuon}, XX GeV $< M_{dimuon} <$ YY GeV
- M_{dijet}
- $M_{missing}$
- N_{pfo}
- $cos(\theta)_{vis}$
- $Angle_{\mu j}$
- M^{recoil}
- $not...HZZ$
- probably more

The detail of the cut efficiency is given in Table**??**.

3.2 Estimation of σ_{ZH}×Br(H→ZZ)

Description of the fitting procedure, fitting figures, and final numbers of the precision.

4 Conclusion

Acknowledgements

Table 1 Overview of the requirements applied for each Higgs decay channels. further explanations should be given here.

Pre-selections		
$N(l) = 2$, where leptons(l) should pass the isolation criteria $N(\mu^+) = 1$, $N(\mu^-) = 1$ with $E(\mu^{\pm}) > 3$ GeV $N(jet) = 2$		
$\mu\mu$H$\nu\nu qq$	$\mu\mu$H$qq\nu\nu$	$\nu\nu$H$\mu\mu qq$
80 GeV $< M_{\mu\mu} <$ 100 GeV	80 GeV $< M_{\mu\mu} <$ 100 GeV	80 GeV $< M_{\mu\mu} <$ 100 GeV
75 GeV $< M_{\mathrm{jj}} <$ 110 GeV	75 GeV $< M_{\mathrm{jj}} <$ 110 GeV	75 GeV $< M_{\mathrm{jj}} <$ 110 GeV
75 GeV $< M_{\mathrm{miss.}} <$ 110 GeV	75 GeV $< M_{\mathrm{miss.}} <$ 110 GeV	75 GeV $< M_{\mathrm{miss.}} <$ 110 GeV
110 GeV $< M_{\mu\mu}^{\mathrm{recoil}} <$ 140 GeV	110 GeV $< M_{\mu\mu}^{\mathrm{recoil}} <$ 140 GeV	110 GeV $< M_{\mathrm{vis.}} <$ 140 GeV
$20 < N_{\mathrm{PFO}} < 90$	$20 < N_{\mathrm{PFO}} < 90$	$20 < N_{\mathrm{PFO}} < 90$
$\lvert\cos\theta_{\mathrm{vis.}}\rvert < 0.95$	$\lvert\cos\theta_{\mathrm{vis.}}\rvert < 0.95$	$\lvert\cos\theta_{\mathrm{vis.}}\rvert < 0.95$
$0° < \Delta\phi_{\mathrm{ZZ}} < 180°$	$0° < \Delta\phi_{\mathrm{ZZ}} < 180°$	$0° < \Delta\phi_{\mathrm{ZZ}} < 180°$
$\left\lvert M_{\mathrm{jj}}^{\mathrm{recoil}} - M^{\mathrm{higgs}}\right\rvert > 3$ GeV	$\left\lvert M_{\mathrm{jj}}^{\mathrm{recoil}} - M^{\mathrm{higgs}}\right\rvert > 3$ GeV	$\left\lvert M_{\mathrm{jj}}^{\mathrm{recoil}} - M^{\mathrm{higgs}}\right\rvert > 3$ GeV
$\nu\nu$H$qq\mu\mu$	qqH$\nu\nu\mu\mu$	qqH$\mu\mu\nu\nu$
80 GeV $< M_{\mu\mu} <$ 100 GeV	80 GeV $< M_{\mu\mu} <$ 100 GeV	80 GeV $< M_{\mu\mu} <$ 100 GeV
75 GeV $< M_{\mathrm{jj}} <$ 110 GeV	75 GeV $< M_{\mathrm{jj}} <$ 110 GeV	75 GeV $< M_{\mathrm{jj}} <$ 110 GeV
75 GeV $< M_{\mathrm{miss.}} <$ 110 GeV	75 GeV $< M_{\mathrm{miss.}} <$ 110 GeV	75 GeV $< M_{\mathrm{miss.}} <$ 110 GeV
110 GeV $< M_{\mathrm{vis.}} <$ 140 GeV	110 GeV $< M_{\mathrm{jj}}^{\mathrm{recoil}} <$ 140 GeV	110 GeV $< M_{\mathrm{jj}}^{\mathrm{recoil}} <$ 140 GeV
$20 < N_{\mathrm{PFO}} < 90$	$20 < N_{\mathrm{PFO}} < 90$	$20 < N_{\mathrm{PFO}} < 90$
$\lvert\cos\theta_{\mathrm{vis.}}\rvert < 0.95$	$\lvert\cos\theta_{\mathrm{vis.}}\rvert < 0.95$	$\lvert\cos\theta_{\mathrm{vis.}}\rvert < 0.95$
$0° < \Delta\phi_{\mathrm{ZZ}} < 180°$	$0° < \Delta\phi_{\mathrm{ZZ}} < 180°$	$0° < \Delta\phi_{\mathrm{ZZ}} < 180°$
$\left\lvert M_{\mathrm{jj}}^{\mathrm{recoil}} - M^{\mathrm{higgs}}\right\rvert > 3$ GeV	$\left\lvert M_{\mathrm{jj}}^{\mathrm{recoil}} - M^{\mathrm{higgs}}\right\rvert > 3$ GeV	$\left\lvert M_{\mathrm{jj}}^{\mathrm{recoil}} - M^{\mathrm{higgs}}\right\rvert > 3$ GeV

Table 2 Summary of event selection.

	$\mu\mu$H$\nu\nu qq$			$\mu\mu$H$qq\nu\nu$			$\nu\nu$H$\mu\mu qq$		
Process	σ[fb]	ϵ[%]	N	σ[fb]	ϵ[%]	N	σ[fb]	ϵ[%]	N
Signal	?	50.0	40						
ZH									
4F									
2F									
	$\nu\nu$H$qq\mu\mu$			qqH$\nu\nu\mu\mu$			qqH$\mu\mu\nu\nu$		
Signal	?	50.0	40						
ZH									
4F									
2F									

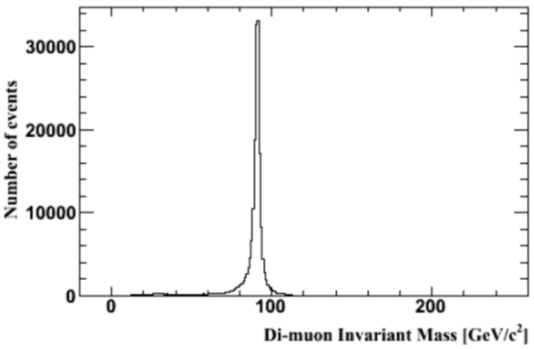

Fig. 2 Dimuon invariant mass distrubution. S+B

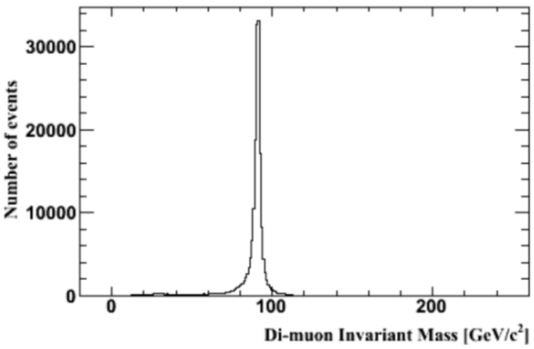

Fig. 3 Dimuon recoil mass distrubution. S+ B

References

1. Author, Article title, Journal, Volume, page numbers (year)

2. Author, Book title, page numbers. Publisher, place (year)

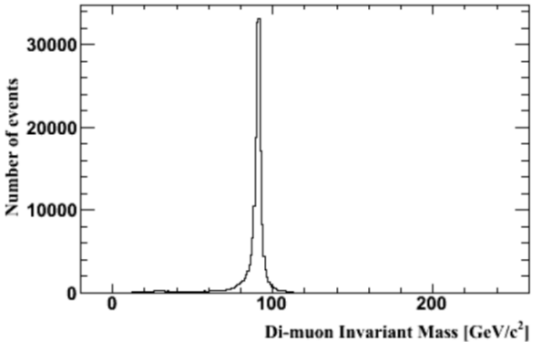

Fig. 4 Npfo distribution. S+B

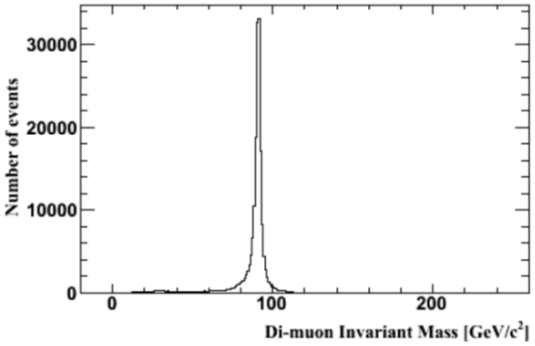

Fig. 5 Cos theta visible distribution. S+B

Table 3 Statistical uncertainties on the product of the ZH cross section and the branching ratio. further explanations should be given here.

Channel		$\frac{\Delta(\sigma \cdot BR)}{(\sigma \cdot BR)}$ [%]
$Z \to \mu^+\mu^-$	$H \to ZZ^* \to \nu\bar{\nu}q\bar{q}$	10.0
$Z \to \mu^+\mu^-$	$H \to ZZ^* \to q\bar{q}\nu\bar{\nu}$	10.0
$Z \to \nu\bar{\nu}$	$H \to ZZ^* \to \mu^+\mu^- q\bar{q}$	10.0
$Z \to \nu\bar{\nu}$	$H \to ZZ^* \to q\bar{q}\mu^+\mu^-$	10.0
$Z \to q\bar{q}$	$H \to ZZ^* \to \mu^+\mu^-\nu\bar{\nu}$	10.0
$Z \to q\bar{q}$	$H \to ZZ^* \to \nu\bar{\nu}\mu^+\mu^-$	10.0
Combined		10.0

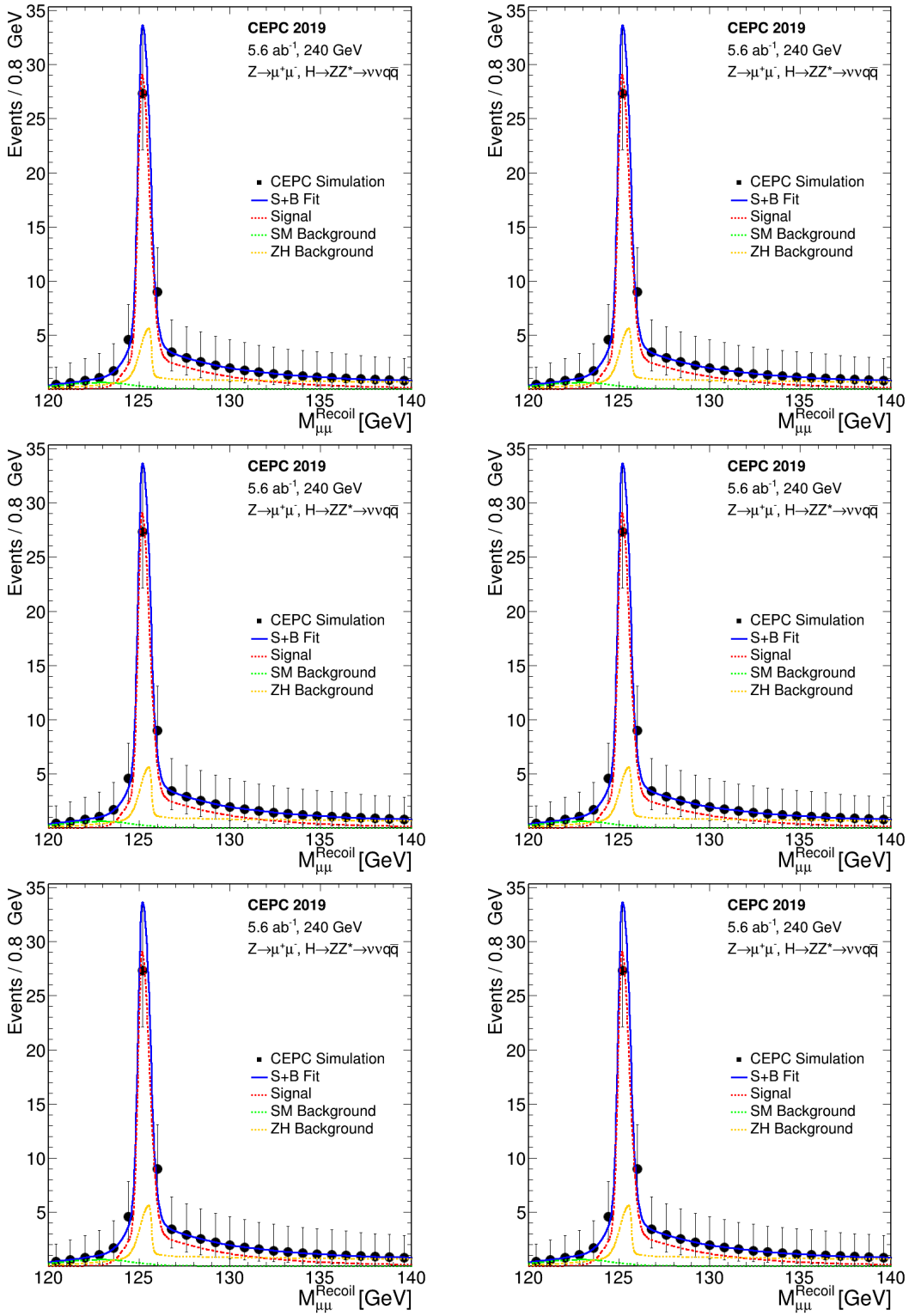

Fig. 6 Recoil mass distributions. further explanations should be given here.